Space Sci Rev (2014) 184:87–106
DOI 10.1007/s11214-014-0097-8

The Energetic Particle Telescope: First Results

V. Pierrard · G. Lopez Rosson · K. Borremans · J. Lemaire · J. Maes · S. Bonnewijn · E. Van Ransbeeck · E. Neefs · M. Cyamukungu · S. Benck · L. Bonnet · S. Borisov · J. Cabrera · G. Grégoire · C. Semaille · G. Creve · J. De Saedeleer · B. Desoete · F. Preud'homme · M. Anciaux · A. Helderweirt · K. Litefti · N. Brun · D. Pauwels · C. Quevrin · D. Moreau · R. Punkkinen · E. Valtonen · W. Hajdas · P. Nieminen

Received: 10 March 2014 / Accepted: 18 August 2014 / Published online: 7 October 2014

Abstract The Energetic Particle Telescope (EPT) is a new compact and modular ionizing particle spectrometer that was launched on 7 May 2013 to a LEO polar orbit at an altitude of 820 km onboard the ESA satellite PROBA-V. First results show electron, proton and helium ion fluxes in the South Atlantic Anomaly (SAA) and at high latitudes, with high flux increases during SEP (Solar Energetic Particles) events and geomagnetic storms. These observations help to improve the understanding of generation and loss processes associated to the Van Allen radiation belts.

V. Pierrard (✉) · G. Lopez Rosson · K. Borremans · J. Lemaire · J. Maes · S. Bonnewijn · E. Van Ransbeeck · E. Neefs
Belgian Institute for Space Aeronomy (BISA), 3 av. Circulaire, 1180 Brussels, Belgium
e-mail: viviane.pierrard@aeronomie.be

V. Pierrard · J. Lemaire · M. Cyamukungu · S. Benck · L. Bonnet · S. Borisov · J. Cabrera · G. Grégoire
Center for Space Radiations, Université Catholique de Louvain (UCL), 2 Chemin du cyclotron, 1348 Louvain-La-Neuve, Belgium

C. Semaille · G. Creve · J. De Saedeleer · B. Desoete · F. Preud'homme
QinetiQ Space, Hogenakkerhoekstraat 9, 9150 Kruibeke, Belgium

M. Anciaux · A. Helderweirt · K. Litefti · N. Brun · D. Pauwels · C. Quevrin · D. Moreau
Belgian User Support and Operations Centre (B.USOC), BISA, 3 av. Circulaire, 1180 Brussels, Belgium

R. Punkkinen
Department of Information Technology, University of Turku, 20014 Turku, Finland

E. Valtonen
Department of Physics and Astronomy, University of Turku, Vesilinnantie 5, 20014 Turku, Finland

W. Hajdas
Laboratory for Particle Physics, Paul Scherrer Institut, OBBA 010, 5232 Villigen, Switzerland

P. Nieminen
ESA, ESTEC European Space & Technology Centre, P.O. Box 299, 2200 AG Noordwijk, The Netherlands

Keywords Van Allen belts · Space radiations · Spectrometer · South Atlantic Anomaly · Solar Energetic Particle events

1 Introduction: The EPT instrument

The Energetic Particle Telescope (EPT) is a new spectrometer that was designed for high-resolution measurements of the charged particle radiation environment in space. Using an innovative concept and the most advanced signal processing technologies, it performs direct electron, proton and heavy ion discrimination over an energy range well beyond that possible with classical particle telescopes, while keeping its high flux measurement capability (Cyamukungu et al. 2011).

The EPT instrument includes (i) a low energy section, consisting of two silicon detectors (one padded front sensor S1/S3 followed by a trigger sensor S2 whose response is treated as in a classical ΔE-E charged particle telescope) and (ii) a high energy section, composed of 10 so-called Digital and Absorber Modules (DAM), each of these comprising a sheet of an absorber material and a silicon sensor (Cyamukungu and Grégoire 2011). These latter sensors are operated in digital mode that means that the only information retained from these sensors is that they are hit or not (signal above a given threshold). Together with energy deposition measurements in the front sensors this gives enough information to identify the type of particle (electron, proton, He ion) and determine its energy. More details about the concept of the EPT can be found in Cyamukungu and Grégoire (2011), and more facts about the EPT configuration that is currently operating onboard PROBA-V can be found in Cyamukungu et al. (2014). Figure 1 shows the instrument whose dimensions are $127.5 \times 162 \times 211.5$ mm^3 and mass is 4.6 kg. The EPT detects the particles penetrating via the aperture cone with an opening angle of 52° (defined by S1/S3 and S2). Due to its modularity, and the novel concept on which EPT has been designed, it is an instrument with customizable maximum energy, field of view angle, geometrical factor, angular resolution and time resolution.

2 Launch and Operation of the PROBA-V Satellite

2.1 The PROBA-V satellite

The first EPT instrument was launched on 7 May 2013 onboard the PROBA-V satellite (Maisongrande et al. 2010) from Kourou in French Guyana with a Vega VV02 rocket. The satellite circulates on a sun-synchronized LEO polar orbit at an altitude of 820 km with an inclination of 98,73° and 10:30 am as nominal local time at the descending node. The orbital rotation period of the satellite is 101.21 minutes. PROBA-V is part of the broader ESA PROBA (PRoject for OnBoard Autonomy) program, described on the ESA website http://www.esa.int/Our_Activities/Observing_the_Earth/Proba-V. Figure 2 shows the small cubic ($765 \times 730 \times 840$ mm, mass: 160 kg) Belgian built ESA satellite PROBA-V, where "V" stands for Vegetation; the body of frame (BOF) axis system is also indicated (The X axis is in the direction of flight and the Z axis is looking towards Earth, the viewing direction of EPT is parallel to the Y axis). The main payload of the satellite is a camera dedicated to the observation of the Earth's vegetation and the EPT as well as a few other instruments were installed onboard as technology demonstration payloads. The satellite is stabilized by magnetic torquers to maintain its orientation with the camera in the direction of the Earth.

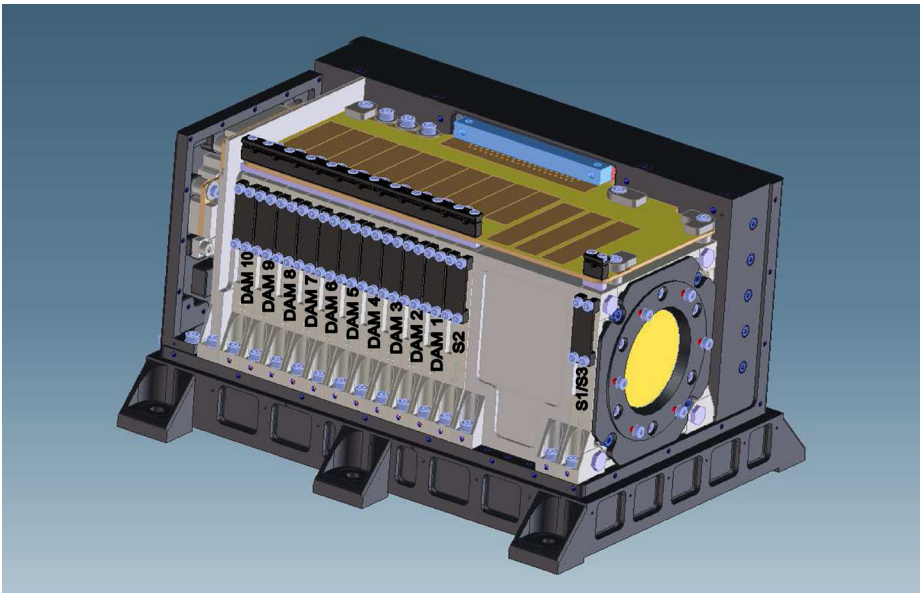

Fig. 1 The EPT instrument without cover and the detector modules labelled (see text)

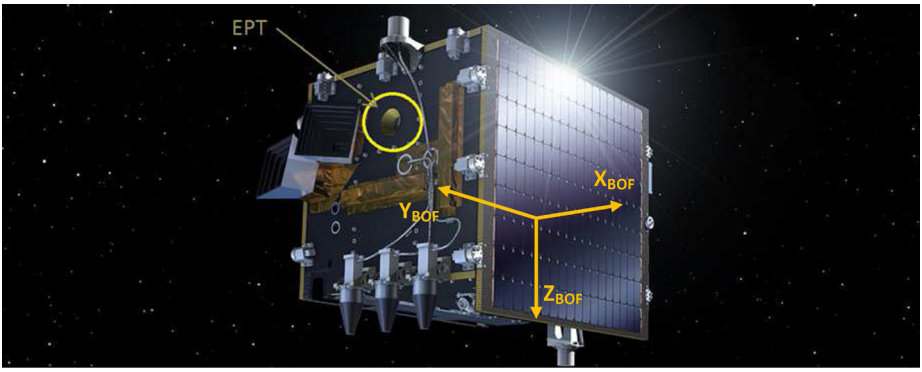

Fig. 2 The satellite PROBA-V including the EPT instrument

The magnetometer that is onboard this satellite measures the three magnetic field components in the BOF reference system which allows defining the boresight orientation of the instrument (field of view direction with respect to the magnetic field) for pitch angle distribution analysis of the measured particle fluxes (the information on the boresight orientation can also be deduced from the calculated magnetic field (IGRF) and the satellite attitude).

2.2 Operations of EPT

The instrument is operated by the B.USOC (Belgian User Support and Operations Centre) acting as the interface between the ESA Redu ground station and the scientists at UCL/CSR. B.USOC is responsible for the acquisition of the raw data from the ground station and for the automatic initial data processing. It provides the scientists at UCL/CSR with an access

Table 1 Energy ranges corresponding to each virtual channel of the EPT instrument for electrons, protons and alpha particles

Energy channels	Electrons (MeV)	Protons (MeV)	Helium ions (MeV)
1	0.5–0.6	9.5–13	38–51
2	0.6–0.7	13–29	51–116
3	0.7–0.8	29–61	116–245
4	0.8–1	61–92	245–365
5	1–2.4	92–126	365–500
6	2.4–8	126–155	500–615
7	8–20	155–182	615–720
8		182–205	720–815
9		205–227	815–900
10		227–248	900–980
11		> 248	> 980

to this data as well as the software needed to perform a manual validation. It serves also as a relay for the on-board configuration of the instrument and provides backup data storage for the processed data. For nominal operations the system is operating fully automatically at B.USOC. An operator and a system support specialist are also available for special cases and emergencies.

Following the commissioning phase, first EPT results have been collected and validated at CSR in UCL (Cyamukungu et al. 2014). The time resolution is adjustable and nominally set to 2 seconds (i.e. the counts registered in the EPT channels are integrated over 2 seconds and full spectra of each particle type is obtained every 2 seconds). The data are corrected and cleaned for possible pile-up in the detectors (Cyamukungu et al. 2014), i.e. unreliable data are flagged in the database. The results show a good coverage of the near-Earth radiation environment with sporadic enhancements caused by Solar Energetic Particle events (SEP) and with high variability due to geomagnetic activity. Data from the EPT will be used to cross-calibrate results obtained from a number of in-orbit radiation monitoring devices with coarser resolution and to characterize the LEO radiation belt fluxes for study of their dynamics and their modelization, for instance to enhance the empirical radiation environment TOP model (Benck et al. 2013).

3 The EPT Data

The EPT instrument measures the particle fluxes of the low altitude radiation belts in 2 (the front sensor is divided into 2 parts) $\times$ 4 (electrons, protons, He^{++}, heavier ions) $\times$ 19 physical channels. The incident spectra (differential flux as a function of energy, treated in terms of so-called virtual channels where each of these is representing an incident energy bin of a given range) are obtained by unfolding the counts in the physical channels with the efficiency matrices (Cyamukungu et al. 2014) of the instrument (obtained for each particle type by GEANT-4 simulations of the instrument under the isotropic flux assumption). Fluxes are provided for 7 virtual channels for electrons, 11 channels for protons and 11 channels for helium ions. Table 1 summarizes the different energy ranges corresponding to each virtual channel.

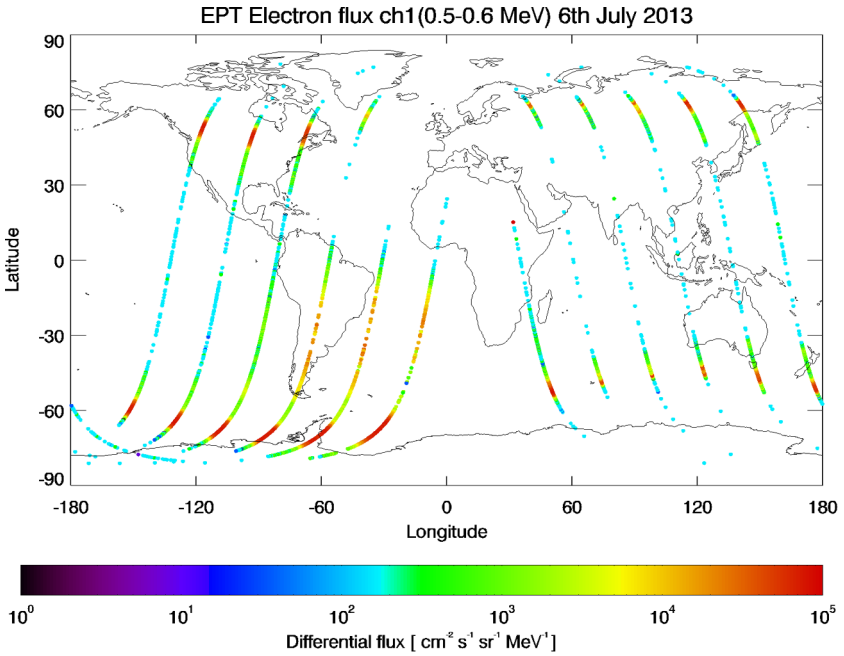

Fig. 3 Electron flux in Channel 1 (500–600 keV) measured during 1-day (6th July 2013) along the orbit of PROBA-V at an altitude of 820 km

3.1 Electron Fluxes

The highest fluxes are observed for low energy electrons (Channel 1). Figure 3 illustrates the electron flux in Channel 1 (500–600 keV) measured during 1-day along the orbit of PROBA-V. The first panel corresponds to the flux observed on July 6, 2013 during a geomagnetic storm with Dst around −80 nT. The fluxes observed during this storm are higher than the fluxes observed during quiet periods, especially at high latitudes.

Figure 4 shows the electron flux in Channel 1 (500–600 keV) accumulated during one month of observations. The first panel corresponds to June 2013 and the second one to July 2013. The fluxes observed during June 2013 are a little bit higher, at high latitudes and in the SAA, because June is a more active period than July 2013. The SAA is well evidenced, as well as the polar "horns" corresponding to the high latitude penetration of the outer belt at low altitudes. The SAA corresponds to the region where the inner Van Allen belt comes closest to the Earth's surface. The magnetic field is weakest in this area, because the intersection between the magnetic and the rotation axis of the Earth is located 500 km further North than the Earth's center. The SAA is located above South America, Atlantic ocean and South Africa for this energy range.

Note also the lower fluxes observed in the Northern hemisphere above the North Atlantic and especially the gap in the Northern horn above Europe. Such low fluxes in the Northern hemisphere were also observed by DEMETER orbiting at an altitude of 700 km (Sauvaud et al. 2008, 2013), as well as by the FEIO detector onboard the SAC-D satellite (S. Bourdarie, personal communication 2014). This is a consequence of the tilt and excentricity of the geomagnetic field line distribution which, at these longitudes, lifts the mirror points of trapped particles at higher altitudes in the Northern hemisphere than in the Southern one where the

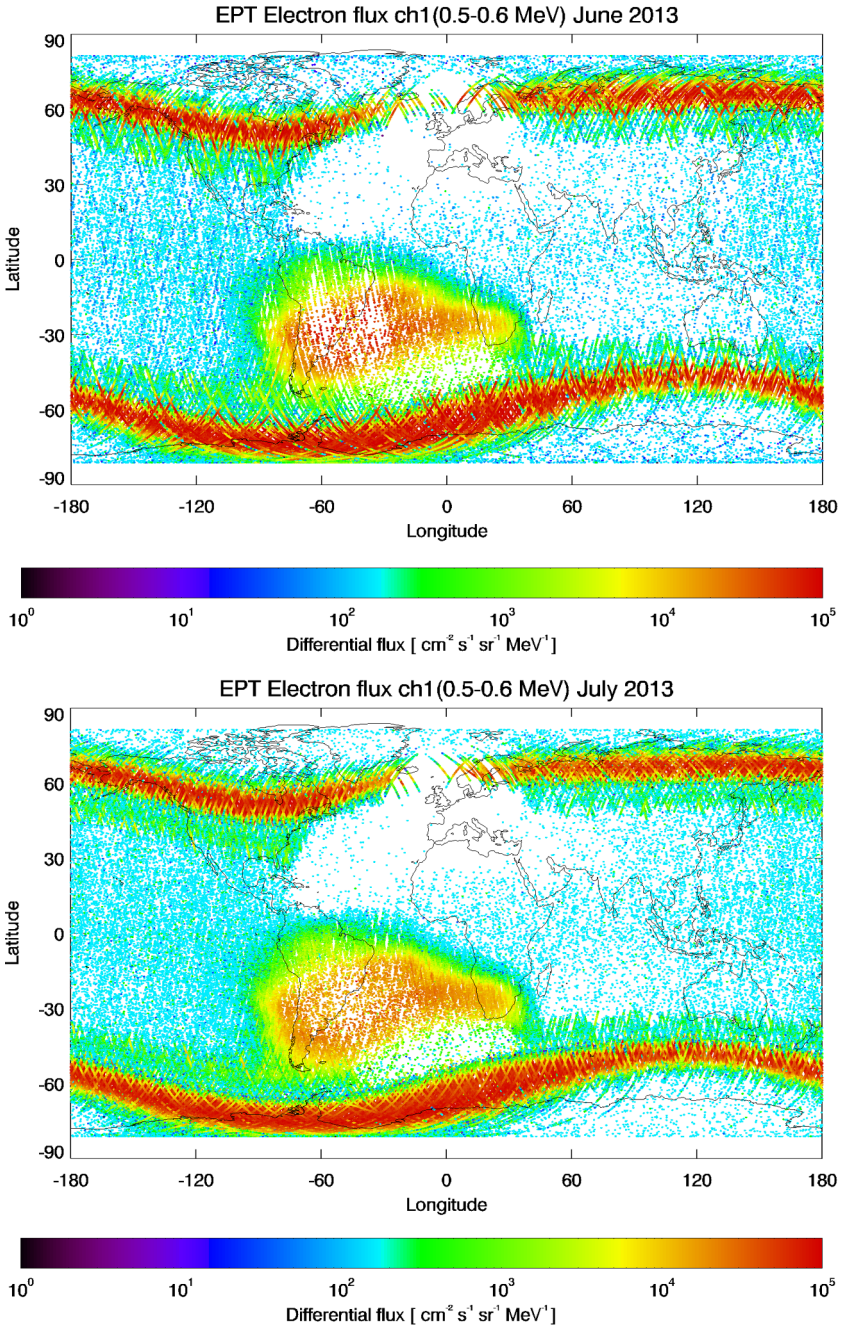

Fig. 4 Electron flux in Channel 1 (500–600 keV) observed during one month of observations. *First panel*: June 2013. *Second panel*: July 2013. One can see the South Atlantic Anomaly (high fluxes), as well as the penetration of the outer belt at high latitudes

surface field intensity is significantly reduced. Because the mirror points are located in the high atmosphere in the Southern hemisphere, the particles are lost and this leads to very low fluxes in the Northern hemisphere above Europe. These low fluxes are not displayed by the AE8 model (Vette 1991) or more recent AE9 model (Ginet et al. 2013) available on SPENVIS (www.spenvis.oma.be).

Figure 5 illustrates the electron flux in Channel 5 (1–2.4 MeV) observed during one month. Again the first panel corresponds to June 2013 and the second panel to July 2013. The fluxes in the SAA are much lower than in Channel 1, and for this energy range, the effect of the higher solar and geomagnetic activity is even more pronounced.

Figure 6 illustrates the electron fluxes in Channel 1 (first panel) and Channel 3 (second panel) observed from May 21, 2013 to January 15, 2014 as a function of McIlwain (1961) parameter L (vertical axis) and time (horizontal axis). McIlwain parameter L (in Earth's radii R_E) corresponds to the equatorial radius of a drift shell in the reference dipole magnetic field.

These plots show the time variations of the fluxes. The inner belt ($L < 2.8$) is detected only when the spacecraft crosses the SAA. The outer belt is much more variable with time. Penetrations of the fluxes at lower L values appear during geomagnetic storms, characterized by minimum values of the Dst index as illustrated on Fig. 6. Four deep minima of Dst appear during this time period: June 1, 2013 (with the minimum Dst $= -119$ nT), June 29, 2013 (with Dst $= -98$ nT) and October 2, 2013 (with Dst $= -67$ nT) and November 9, 2013 (with Dst $= -81$ nT). It can be seen that the main geomagnetic storms correspond to injections of electrons at lower L values.

The red dots in the first panel of Fig. 6 correspond to Solar Energetic Particle (SEP) events observed from the launch of EPT in May 2013 up to January 15, 2014. Six main SEP events were observed: May 22, 2013 (with maximum on May, 23) due to asymmetric halo, June 23, 2013 due to a Coronal Mass Ejection (CME), September 30, 2013 due to a CME with erupting filament and December 28, 2013 due to another CME, and January 6 and 9, 2014 (again due to asymmetric halo) (source: http://umbra.nascom.nasa.gov/SEP/). During such SEP events, particles emitted by the Sun are accelerated to very high energies due to a solar flare or shocks associated with coronal mass ejections (CME) and arrive to the Earth with speeds close to that of light. The solar plasma associated to a CME can also cause geomagnetic storms a few days later when it reaches the magnetosphere, as for example the case of the CME on 30 September 2013 and the geomagnetic storm on 2nd October 2013.

Figure 7 shows MagEIS data from the RBSP or Van Allen Probe B covering the same time period and very similar channel energies. The fluxes in the outer belt show similar variations as a function of geomagnetic activity. They are more intense in the Probe data as expected since the RBSP orbit near the equatorial plane. Note that in the inner zone, what appear to be significant fluxes of energetic electrons is due to background from energetic protons. Due to the novel concept of the EPT design its data don't suffer of similar contamination.

Similar comparisons have been made with SAC-D that has also a LEO orbit (670 km for SAC-D) and RBSP-A. The same variations with geomagnetic activity are also observed.

Figure 8 shows the comparison between the EPT observations at $6.5 < L < 7$ for Channel 1 (500–600 keV) averaged on 10 minutes with GOES15 in situ observations (475 keV) at the geostationary orbit. The GOES fluxes are systematically higher, as these data are acquired close to the geomagnetic equator and the nominal energy is somewhat lower, but similar temporal variations are observed as a function of geomagnetic activity.

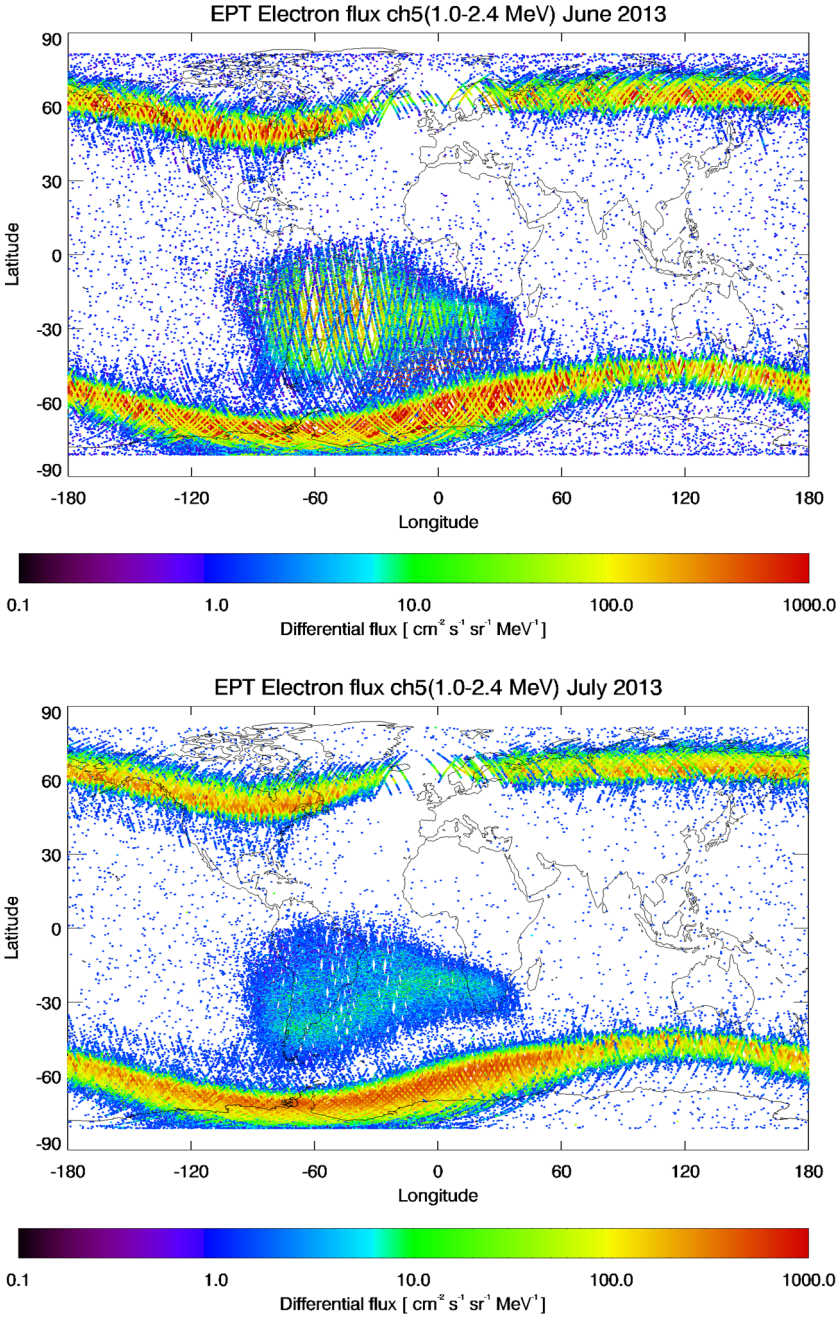

Fig. 5 Electron flux in Channel 5 (1–2.4 MeV) observed during one month of observations. *First panel*: June 2013. *Second panel*: July 2013

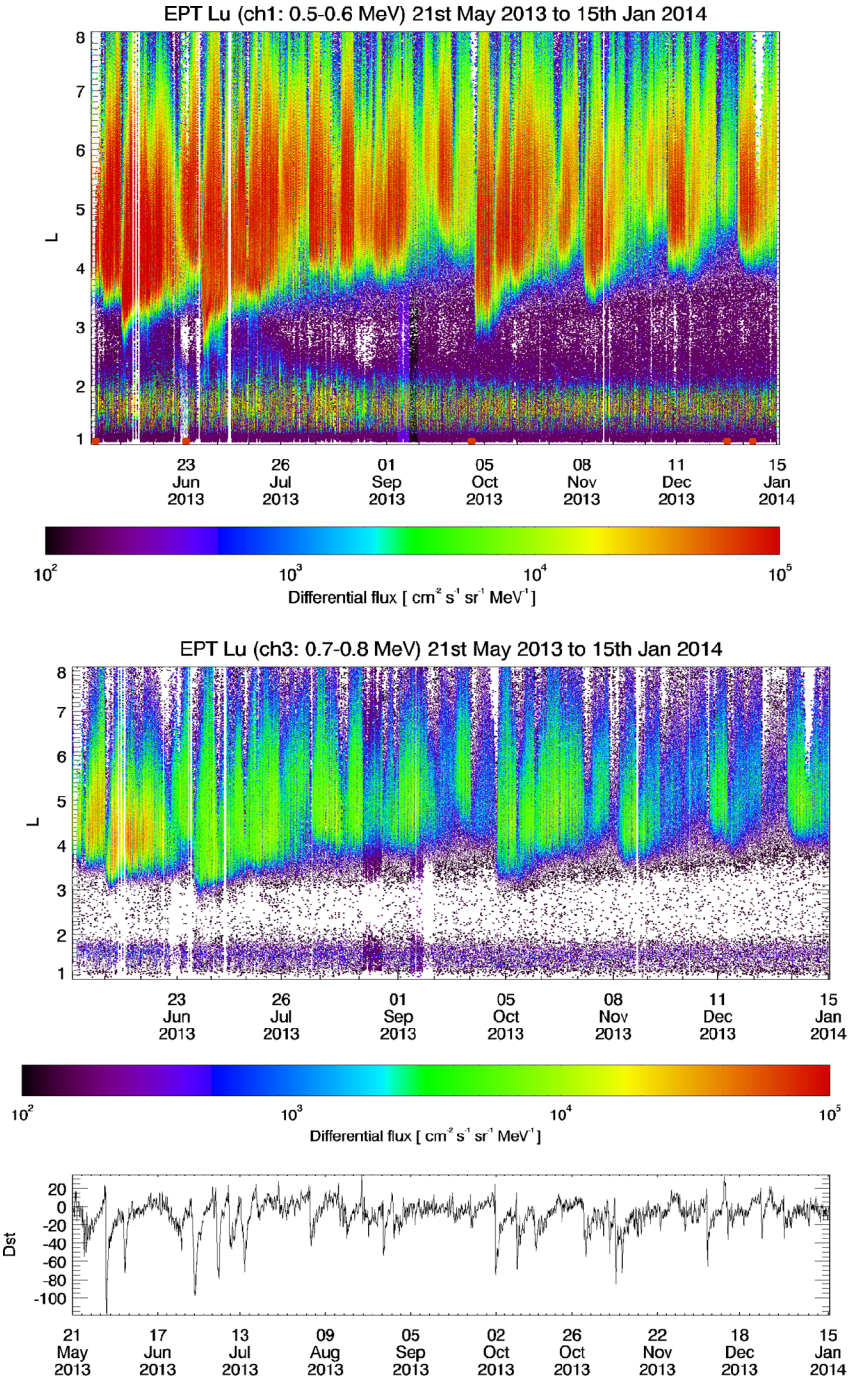

Fig. 6 Electron fluxes observed by EPT from May 21, 2013 up to January 15, 2014 as a function of the McIlwain parameter *L* (*vertical axis*) and time (*horizontal axis*) for Channel 1 (*first panel*) and Channel 3 (*second panel*) using the same color scale. Dst (Disturbed Storm Time) index measured from May 21, 2013 to January 15, 2014 is given in *panel 3*

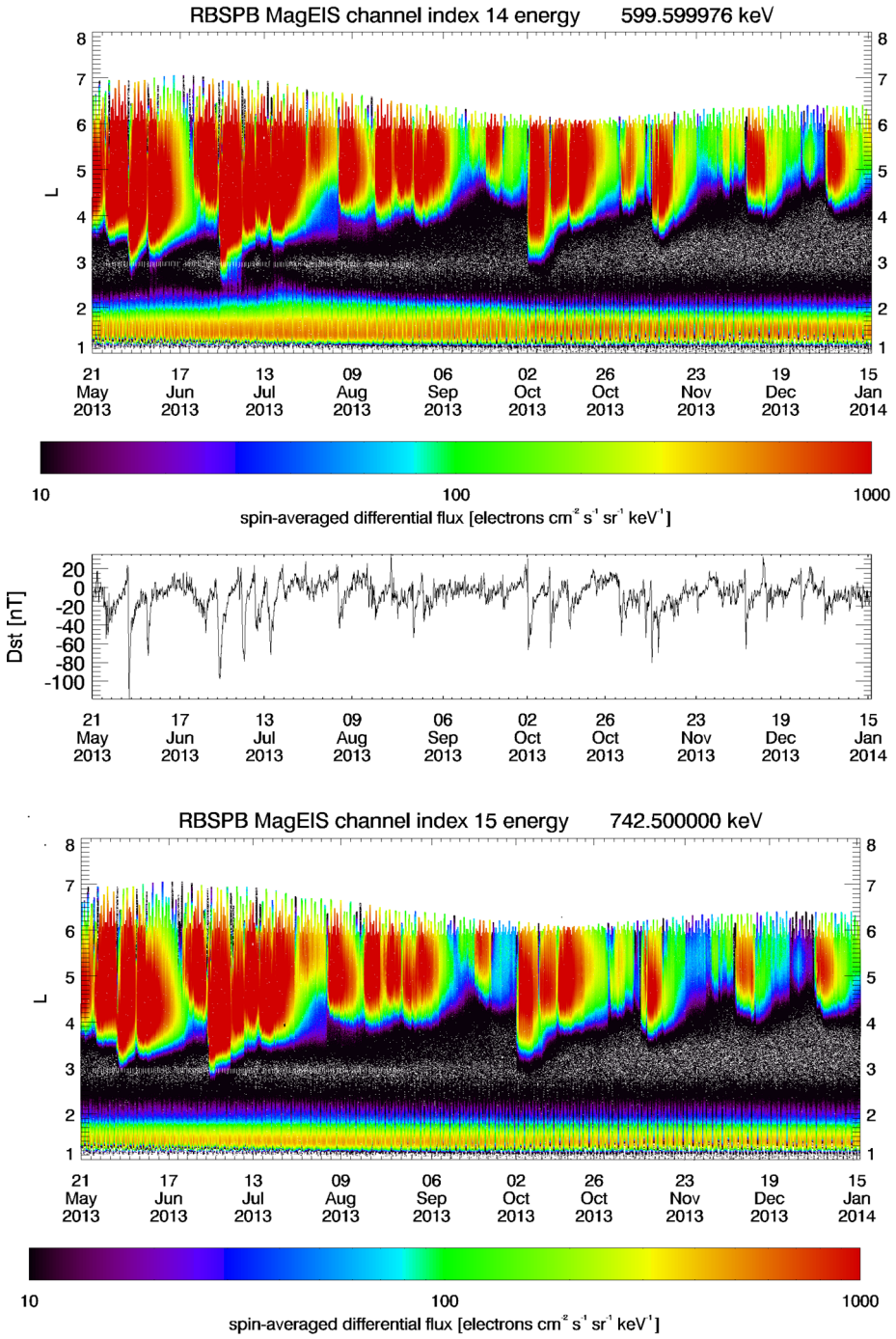

Fig. 7 Electron fluxes as a function of L and time, observed by Mageis onboard Van Allen Probe B from May 21, 2013 to January 15, 2014: 600 keV electrons (*upper panel*) and 742.5 keV electrons (*bottom panel*)

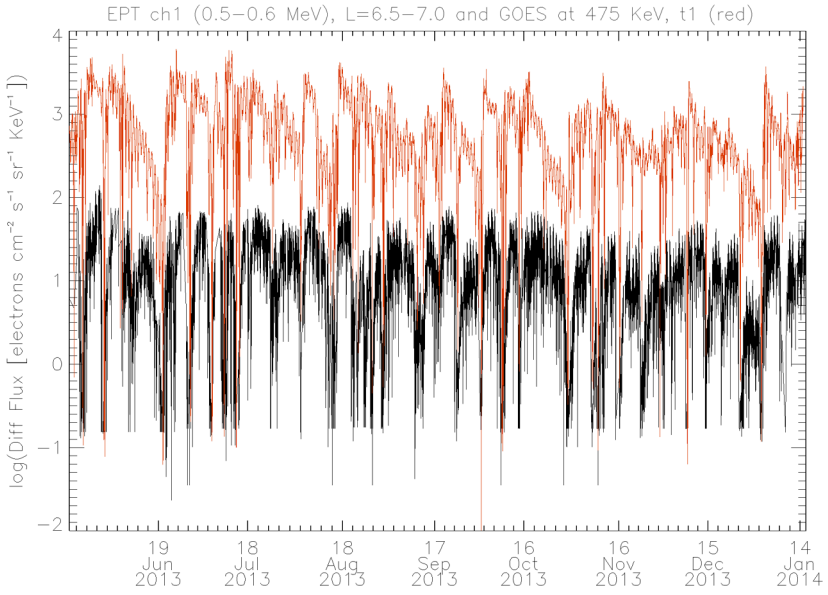

Fig. 8 GOES15 (MAGED instrument, Telescope 1) in situ observations of electron fluxes (*red*) at geostationary orbit for $E = 475$ keV compared to EPT (*black*) in the energy range 500–600 keV, between $L = 6.5$ and 7, for the same time period

3.2 Proton Fluxes

Proton fluxes along one-day orbits of the PROBA-V satellite are generally detected only in the SAA. At high latitudes, the proton fluxes do not penetrate down to 820 km of altitude, except during SEP events. This is illustrated by Fig. 9 for the SEP of 23 May. High latitude fluxes are till detected on 24 May, but have already decreased.

Figure 10 shows the proton fluxes in Channel 1 (9.5–13 MeV) observed during one month. The first panel corresponds to June 2013 and the second one to September 2013 when a SEP event is observed at the end of the month on 30 September. The South Atlantic Anomaly is well prominent. High latitude fluxes are only visible during the day of the SEP events (i.e. 23 June for panel 1 and 30 September for the second panel) and the following day. That is why the orbit of the spacecraft is then well visible for these high latitude fluxes. Note the unusual band visible in the Southern hemisphere around 60° (and also partially in the Northern hemisphere) in June 2013. This band around −60° of latitude is also observed during the same period of time in Channels 2 and 3, but not in Channels 4–6. It is not observed during other months, as shown by the second panel for September 2013.

Similar bands have been observed in the standard proton detector of the POES mission, and have been interpreted as contamination due to energetic outer belt electron. Figure 11 shows the proton map observed by POES on a similar orbit (840 km of altitude, inclination 98°). It shows the omnidirectional flux for protons with energies higher than 16 MeV from 20 May 2013 up to 31 January 2014.

As with EPT, proton fluxes are observed at high latitudes only during SEP events. The structure located between the SAA and the south horn appears also in these POES observations, as in EPT during June 2013 after a SEP event. Such band of proton precipitation at higher L in the southern hemisphere were also reported by Evans et al. (2008) after two SEP

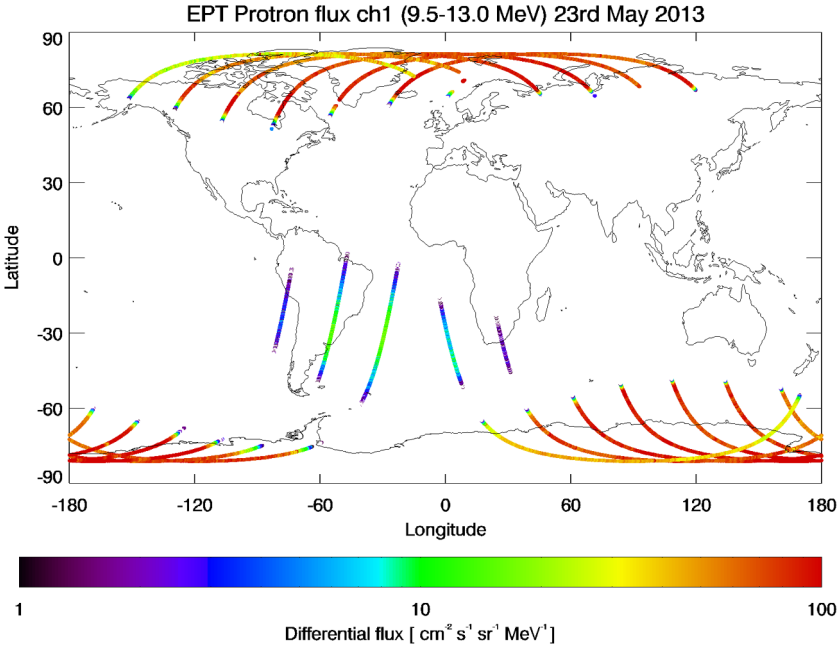

Fig. 9 Proton fluxes measured in Channel 1 (9.5–13 MeV) along the orbit of PROBA-V satellite on May 23, 2013 during the SEP event that started on May 22, 2013

events on the 1st of November and the 10th of November 2004. However, Evans et al. 2008 stated that a careful analysis of the POES proton data set indicated that the high latitude flux enhancement (northern and southern bands) they observed after SEP events in late 2004 and early 2005, was likely due to $E > 3$ MeV electrons and not due to high energy protons.

With EPT, it is noted also that the appearance of these protons in location and intensity is correlated to the high energy electron flux above 2 MeV. It must be stated that the data until 24 June has been acquired during the commissioning phase of the EPT and that the EPT was not running with its optimal configuration. This means that the energy deposition limits set for each analogue detector S1, S2 and S3 to define the various detection channels, were not yet optimized. While it was definitely observed that with the un-optimized configuration particle type misidentification could occur, contamination under the optimized configuration was found to be extremely negligible, since the channel definition process excluded recording of particles with ambiguous signature. For instance, the EPT identification of particles in the HES, requires cross validation from both the S2 and the S1/S3 sensors (Cyamukungu et al. 2014).

GEANT4 simulations showed that with the unoptimized configuration file, electrons can be registered as 29–61 MeV (Channel 3) protons if their energy is above 2 MeV, but it needs a flux of ~ 400 electrons/cm^2/s/sr/MeV in the energy range 2.4–8 MeV, to register 1 event in the corresponding proton channel. At the time of this unusual proton occurrence, sometimes more than 10 counts could be registered in this proton channel and the highest flux observed for 2.4–8 MeV electrons was around 200 #/cm^2/s/sr/MeV. With the more restricted energy limits for particle identification (configuration file after 24 June 2013), the electron contamination efficiency was calculated to be zero. After optimization of the EPT

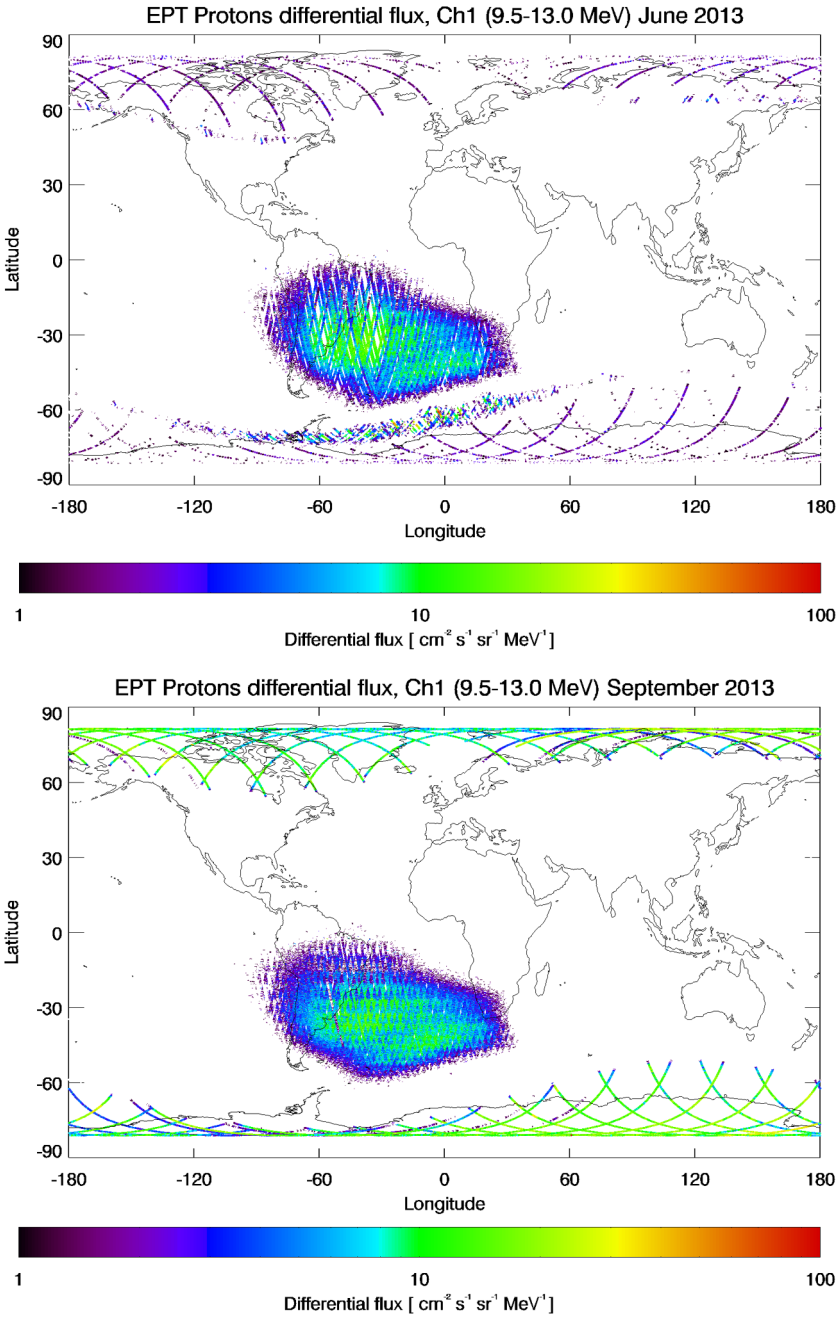

Fig. 10 Proton flux in Channel 1 (9.5–13 MeV) observed during one month of observations. *First panel*: June 2013, *second panel*: September 2013

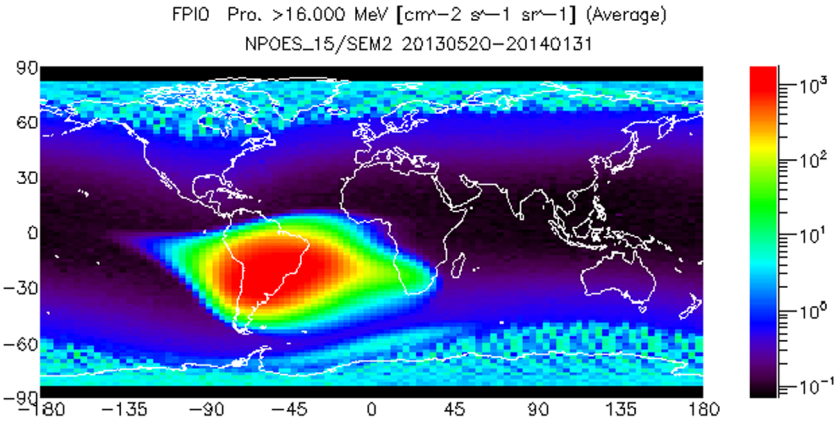

Fig. 11 POES proton observations for $E > 16$ MeV from 20 May 2013 up to 31 January 2014

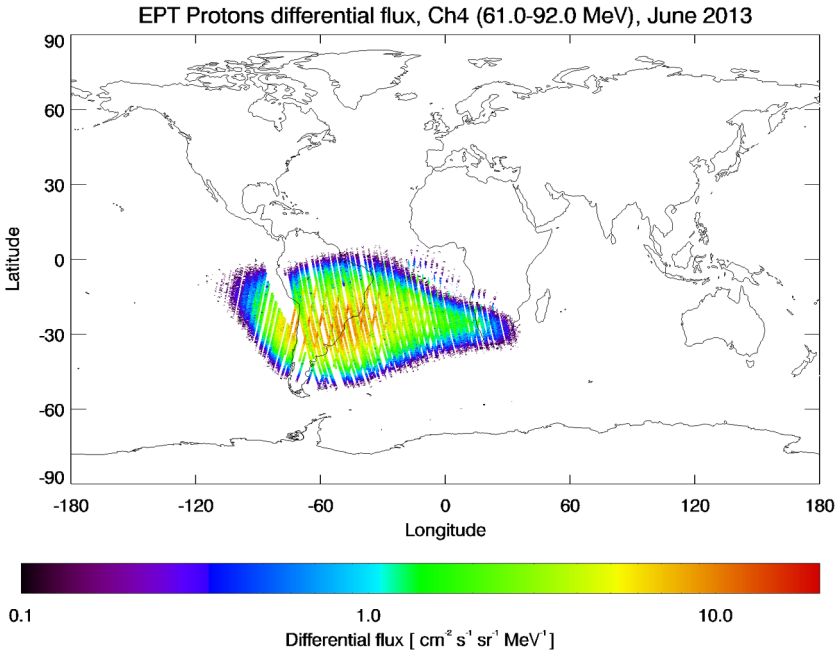

Fig. 12 Proton flux in Channel 4 (61–92 MeV) observed during the month of June 2013 (only with pitch angles between 80 and 100°)

configuration, no such intense high latitude proton population was observed anymore, but the May SEP event was also the strongest one since launch of EPT.

Figure 12 illustrates directional proton fluxes from Channel 4 during the month of June 2013 using only the measurements with boresight orientation between 80° and 100°. The omnidirectional flux divided by 4π gives a good estimation (within a factor of about 2) of the proton directional flux for the covered particle pitch angle range (Cabrera et al. 2005). At low altitudes, the high-energy trapped proton fluxes are strongly anisotropic, i.e. proton

fluxes depend on their arrival direction in the plane perpendicular to the local magnetic field vector, as well as on their pitch angle. The anisotropy manifests itself through steep pitch angle distributions and the so-called East-West effect: The pitch angle distribution is due to the particle gyration around magnetic field lines and their mirroring in an inhomogeneous magnetic field. The East-West effect is the result of the interaction of the protons with the Earth's magnetosphere.

Below 2000 km, the gyroradii of trapped protons with energies above 1 MeV are comparable to the neutral atmospheric scale height, which means that during a gyration they encounter different atmospheric densities and this causes differences of a factor of three or more in fluxes arriving from different azimuths (Kruglanski 1996). Due to the orientation of the PROBA-V satellite, dayside measurements correspond to westward fluxes, while nightside measurements correspond to eastward fluxes. Due to their wider pitch angle distributions and the wider field of view the electrons can be assumed almost omnidirectional, at least in first order approximation (Cyamukungu and Grégoire 2011).

Figure 13 illustrates the proton fluxes observed from May 21, 2013 to January 15, 2014 as a function of L (vertical axis) and time (horizontal axis) for Channel 1 (first panel) and Channel 3 (second panel) using different color scales. The red dots in the bottom panel correspond to the main SEP events. One can see that each SEP event corresponds to the injection of energetic protons on distant drift shells. The particles penetrate the Earth's magnetic field into the polar regions. The injected proton fluxes remain high for several days after the event. Note that after the SEP event of 22 May, particles remain trapped at $L = 4$–5 during more than one month (up to July) and form the additional proton belt displayed on Fig. 10 (upper panel) corresponding to the month of June. There are almost no fluxes outside the SAA from July to 30 September 2013.

3.3 Helium Fluxes

Figure 14 illustrates the Helium fluxes observed in Channel 1 when accumulated from 16 May to 21 October 2013. Almost no measurable He^{++} ion fluxes are observed on individual orbits except during SEP events, when the fluxes at high latitudes are higher than 0.01 He^{++} cm^{-2} s^{-1} sr^{-1} MeV^{-1}. EPT observations show very low fluxes in the SAA.

Figure 15 shows that injections of helium ions appeared during the SEP events (again identified by the red dots on the x axis) at $L > 4.5$, but they disappear after one day.

4 Discussion, Conclusions and Perspectives

The new spectrometer EPT measures directional fluxes of electrons, protons and heavier ions simultaneously in different energy ranges. This enables us to produce world maps of electron fluxes between 0.5 and 20 MeV, proton fluxes between 9.5 and 300 MeV and helium fluxes between 38 MeV and 1600 MeV. Due to the widely varying fluxes of electrons, protons and heavy ions within the radiation belts, the instrument was designed with a unprecedented in-flight particle and energy discrimination capability that provides more precise measurements than those made by previous detectors which have been used in the past to build the AE8, AP8, AE9, AP9 and other empirical radiation belt models. The results of the EPT will now be available for the development of more elaborated statistical models of the space radiation environment.

The simultaneity of the energetic electron, proton and helium ion flux measurements is also an unprecedented asset of the EPT detector.

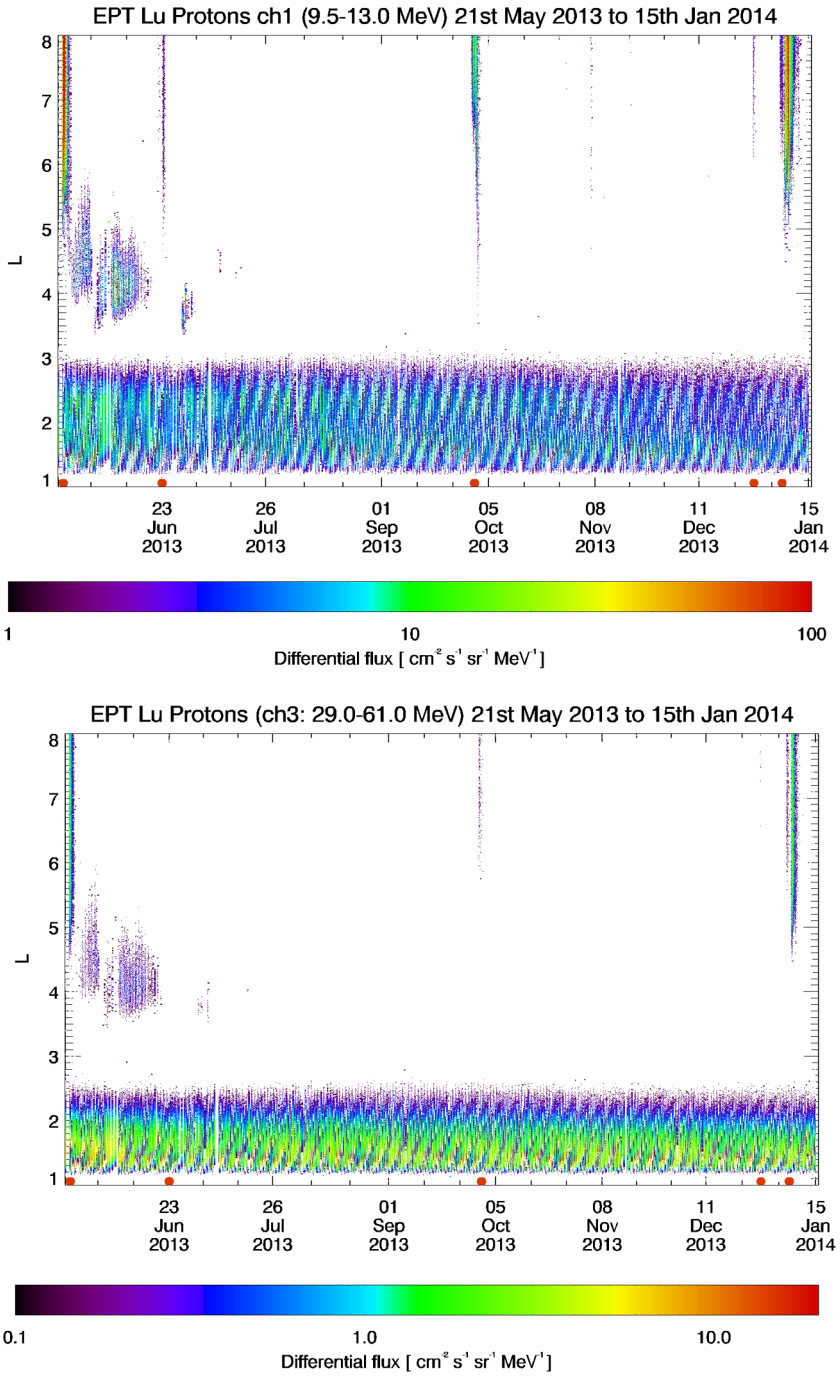

Fig. 13 Proton fluxes observed from May 21, 2013 up to January 15, 2014 as a function of L (*vertical axis*) and time (*horizontal axis*) for Channel 1 corresponding to 9.5–13 MeV (*first panel*) and Channel 3 corresponding to 29–61 MeV (*second panel*). Note that different *color scales* are used for both panels

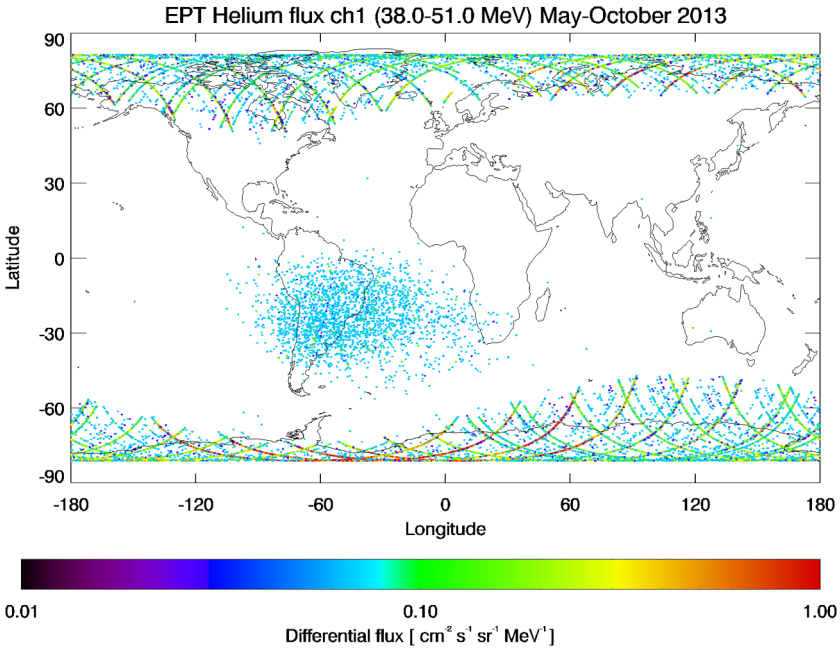

Fig. 14 Helium fluxes observed in Channel 1 when accumulated from 16 May to 21 October 2013

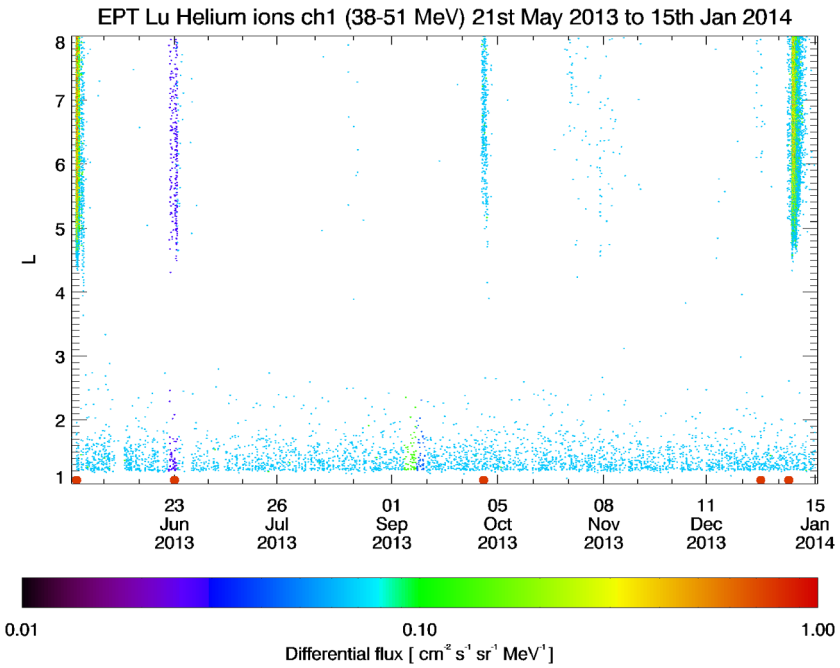

Fig. 15 Helium fluxes observed from May 21, 2013 to January 15, 2014 as a function of L (*vertical axis*) and time (*horizontal axis*) for Channel 1

First EPT observations show electron, proton and helium ion fluxes in the South Atlantic Anomaly (SAA), as well as at high latitudes, with significant flux enhancements during SEP events in the polar regions. These yet unforeseen enhancement will need further investigations and a proper theory to account for their injection into the Radiation Belts drift shells.

An important difference with the fluxes predicted by the AE8 and AE9 model was found in the magnetically conjugate region of the SAA in the Northern hemisphere where the IGRF magnetic field has a relatively pronounced maximum and where very low fluxes are observed in Figs. 4 and 6. The extension and shape of the SAA is also somewhat different from that predicted by the AE8 and AP8 model in some energy ranges. Indeed, due to the secular variation of the IGRF, the epicenter of the SAA has moved westward at a rate of 0.3 deg/year between the early radiation belt measurements in the 60's and the present epoch (Heynderickx 1996).

Flux variations observed by EPT allow us to better understand the dynamics of the radiation belts, especially during Solar Energetic Particle (SEP) events, as well as during other changes of Interplanetary Magnetic Field (IMF) and geomagnetic field. Losses and sources of relativistic electrons in the outer belt have been recently reviewed by Shprits et al. (2008a, 2008b). These source and loss processes are controlled by radial transport, as well as by local acceleration due to different waves. Radiation belt electron precipitation due to whistler waves of ground-based VLF transmitters have also been reported at such low altitudes (Vampola 1977; Sauvaud et al. 2008).

The worldwide distribution of the protons at 820 km altitude can also be determined and modeled from the EPT uncontaminated energy spectra of the electrons, protons, and He^{++} ions collected already since May 2013. Indeed, the instrument provides uncontaminated spectra well discriminated for each particle species unprecedented energy resolution and very good time resolution (2 s). EPT spectra can be compared with AE8 and AP8 models (Pierrard and Lemaire 1996; Pierrard and Borremans 2012) and with the low altitude trapped proton model for solar minimum conditions based on SAMPEX/PET data that was developed some years ago (Heynderickx et al. 1999; Pierrard et al. 2000). There are also other RB measurements from LEO missions (POES, EQUATOR-S, DEMETER, SAC-D, ...) which had energetic particle detectors/spectrometers onboard, and that can be cross-calibrated a posteriori using the uncontaminated EPT energy spectra.

Significant proton flux enhancements during SEP events are observed by the EPT instrument. It appears definitely from EPT data that the main time variations of proton and helium fluxes at 820 km are associated with SEP events. Relativistic electrons injections are also associated with SEP events (on May 23 and September 30, 2013 for instance), but also with Dst geomagnetic storms.

The EPT observations will be used to complete the empirical dynamic model of the space radiations to predict the flux variations during geomagnetic storms at LEO orbit (Benck et al. 2010, 2013). Actually this model is based on data of DEMETER (Sauvaud et al. 2008, 2013) and SAC-C that have been registered during the last solar cycle maximum and declining phase (2000–2006). Cluster observations have also been analyzed to determine the flux variations during geomagnetic storms. The Cluster spacecraft, as well as RBSP, directly cross the middle of the radiation belts and complete the observations of LEO satellites.

Dynamic simulations based on averaged Cluster observations have been developed to give the flux of non-relativistic electrons during quiet and storm time periods. Using simultaneous observations of the Cluster instruments RAPID, CIS and WHISPER, Pierrard and Benck (2012) and Darrouzet et al. (2013) showed also observed links between the position of the plasmapause and the locations of the electron radiation belts boundaries for different energies. Cluster spacecraft continue to provide observations that can be compared with

EPT. The two Van Allen Probes launched by NASA in 2012 provide also high resolution measurements in the heart of the radiation belts that are compared with EPT observations.

Unlike many solid state detectors used since the 60's to measure the fluxes of energetic charged particles in the Earth's radiation belts, the energy channels of the EPT are free of contamination from fluxes of other (undesired) types of penetrating particles. This is an advantage of the novel concept on which this new solid state detector/spectrometer is based.

In the future, the EPT instrument could be implemented on other spacecraft to measure the space radiation fluxes. As a consequence of the modularity of the EPT instrument, its energy ranges, its sizes, and mass can easily be adapted to the needs of future GEO, GTO, as well as other LEO space missions.

Acknowledgements V. Pierrard and the Space Physics Department of BISA thank the Belgian Science Policy—Space Research and Applications (Belspo) for the supplementary researcher program entitled "Scientific analysis of EPT (Energetic Particle Telescope) measurements". The research leading to these results has also received funding from the European Union's Seventh Programme for Research, Technological Development and Demonstration under Grant Agreement n°263340 SWIFF (www.swiff.eu) and was subsidized by the Scientific Federal Policy in the framework of the program Interuniversity Attraction Pole for the project P7/08 CHARM.

The development of the EPT instrument was realized with the support of the Belspo and of the European Space Agency (ESA) (contracts 20294/06/NL/JD (Phase A/B) and 22582/09/NL/AT (Phase C/D)). The design of the EPT instrument and its integration on the PROBA-V satellite results from a fruitful Consortium between the Université Catholique de Louvain, the Belgian Institute for Space Aeronomy and QinetiQ Space. The B.USOC and the control center in Redu provide data transmission and storage. The authors thank all the scientists who temporarily participated to the development of the EPT instrument and its integration on PROBA-V satellite, as well as the administrative teams of the different institutes. The CSR team also thanks Belspo for supporting the "PROBA-V/EPT – Data Exploitation" project via the PRODEX program under ESA contract C4000107617) and for the PRODEX-7 (N° 90098+ CCN-1/C 90098). They also thank G. Tabordon, L. Kruijfthooft, C. Thielens, B. de Callatay and the radioprotection and cyclotron teams. EPT data can be consulted on the website http://web.csr.ucl.ac.be/csr_web/probav/index.html.

The authors thank the reviewers for their suggestions to improve the manuscript, especially for the comparisons with Van Allen Probes. The authors thank also Drs S. Bourdarie and V. Maget from ONERA in Toulouse (France) for providing the observations of SAC-D and POES that were used for comparisons with EPT measurements and for many useful discussions to improve the analysis of the data.

References

S. Benck, L. Mazzino, M. Cyamukungu, J. Cabrera, V. Pierrard, Low altitude energetic electron lifetimes after enhanced magnetic activity as deduced from SAC-C and DEMETER data. Ann. Geophys. **28**, 848–859 (2010). www.ann-geophys.net/28/849/2010/

S. Benck, M. Cyamukungu, J. Cabrera, L. Mazzino, V. Pierrard, The Transient Observation-based Particle (TOP) model and its potential application in radiation effects evaluation. J. Space Weather Space Clim. **3**, 1–10 (2013). doi:10.1051/SWSC/2013024

J. Cabrera, M. Cyamukungu, P. Stauning, A. Leonov, P. Leleux, J. Lemaire, G. Grégoire, Fluxes of energetic protons and electrons measured on board the Oersted satellite. Ann. Geophys. **23**, 2975–2982 (2005). doi:10.5194/angeo-23-2975-2005

M. Cyamukungu, G. Grégoire, The Energetic Particle Telescope (EPT) concept and performances, in *Proc. SPIE*, vol. 8148, Solar Physics and Space Weather Instrumentation IV (2011), 814803. doi:10.1117/12.892420

M. Cyamukungu, S. Benck, I. Brivitch, W. Hajdas, G. Santin, A. Zadeh, A. Meniucci, P. Nieminen, R. Punkkinen, E. Valtonen, C. Semaille, B. Desoete, J. De Saedeleer, G. Creve, E. Van Ransbeeck, J. Maes, S. Bonnewijn, G. Grégoire, J. Cabrera, Perspectives for provision of high quality space radiation environment data using the Energetic Particle Telescope (EPT), in *RADECS 2011*, ed. by J. Schwank (Institute of Electrical and Electronics Engineers, 2011), pp. 569–572. doi:10.1109/RADECS.2011.6131438

M. Cyamukungu, S. Benck, S. Borisov, G. Grégoire, J. Cabrera, J.-L. Bonnet, B. Desoete, F. Preud'homme, C. Semaille, G. Creve, J. De Saedeleer, S. Ilsen, L. De Busser, V. Pierrard, S. Bonnewijn, J. Maes, E. Van Ransbeeck, E. Neefs, J. Lemaire, E. Valtonen, R. Punkkinen, M. Anciaux, K. Litefti, N. Brun, D.

Pauwels, C. Quevrin, D. Moreau, A. Helderweirt, W. Hajdas, P. Nieminen, The Energetic Particle Telescope (EPT) on board PROBA-V: description of a new science-class instrument for particle detection in space. IEEE Trans. Nucl. Sci. (2014, submitted)

F. Darrouzet, V. Pierrard, S. Benck, G. Lointier, J. Cabrera, K. Borremans, N. Ganushkina, J. De Keyser, Links between the plasmapause and the radiation belts boundaries as observed by the instruments CIS, RAPID and WHISPER on CLUSTER. J. Geophys. Res. **118**, 4176–4188 (2013). doi:10.1002/jgra.50239

D. Evans, H. Garett, I. Jun, R. Evans, J. Chow, Long-term observations of the trapped high-energy proton population ($L < 4$) by the NOAA Polar Orbiting Environmental Satellite (POES). Adv. Space Res. **41**, 1261–1268 (2008)

G.P. Ginet, T.P. O'Brien, S.L. Huston, W.R. Johnston, T.B. Guild, R. Friedel, C.D. Lindstrom, C.J. Roth, P. Whelan, R.A. Quinn, D. Madden, S. Morley, Y.-J. Su, AE9, AP9 and SPM: new models for specifying the trapped energetic particle and space plasma environment. Space Sci. Rev. **179**(1–4), 579–615 (2013). doi:10.1007/s11214-013-9964-y

D. Heynderickx, Comparison between methods to compensate for the secular motion of the South Atlantic Anomaly. Nucl. Tracks Radiat. Meas. **26**, 325–331 (1996)

D. Heynderickx, M. Kruglanski, V. Pierrard, J. Lemaire, M.D. Looper, J.B. Blake, A low altitude trapped proton model for solar minimum conditions based on SAMPEX/PET data. IEEE Trans. Nucl. Sci. **46**, 1475–1480 (1999)

M. Kruglanski, Engineering tool for trapped proton flux anisotropy evaluation. Radiat. Meas. **26**, 953 (1996)

P. Maisongrande, J. Vandenabeele, J.-P. Malingreau, A. Lobo, P. de Fourny, E. Gonthier, K. Mellab, R. Kleihorst, PROBA-V, a satellite for the continuity of the SPOT/VEGETATION mission. Geophys. Res. Abstr. **12**, EGU2010-14202-1 (2010)

C.E. McIlwain, Coordinates for mapping the distribution of magnetically trapped particles. J. Geophys. Res. **66**, 3681–3691 (1961)

V. Pierrard, S. Benck, The dynamics of the terrestrial radiation belts and its links to the plasmasphere, in *Space Weather: the Space Environment*. AIP Conf. Proc., vol. 1500 (2012), p. 216. doi:10.1063/1.4768769

V. Pierrard, K. Borremans, Fitting the AP8 spectra to determine the proton momentum distribution functions in space radiations. Radiat. Meas. **47**, 401–405 (2012). doi:10.1016/j.radmeas.2012.04.002

V. Pierrard, J. Lemaire, Fitting the AE-8 energy spectra with two maxwellian functions. Radiat. Meas. **26**(3), 333–337 (1996)

V. Pierrard, J. Lemaire, D. Heynderickx, M. Kruglanski, M. Looper, B. Blake, D. Mewaldt, Statistical analysis of SAMPEX/PET proton measurements. Nucl. Instrum. Methods Phys. Res. **449**, 378–382 (2000)

J.-A. Sauvaud et al., Radiation belt electron precipitation due to VLF transmitters: satellite observations. Geophys. Res. Lett. **35**, L09101 (2008). doi:10.1029/2008GL033194

J.-A. Sauvaud et al., Inner radiation belt particle acceleration and energy structuring by drift resonance with ULF waves during geomagnetic storms. J. Geophys. Res. **118**, 1723–1736 (2013). doi:10.1002/jgra.50125

Y.Y. Shprits, S.R. Elkington, N.P. Meredith, D.A. Subbotin, Review of modeling of losses and sources of relativistic electrons in the outer belt I: radial transport. J. Atmos. Sol.-Terr. Phys. **70**, 1679–1693 (2008a). doi:10.1016/j.jastp.2008.06.008

Y.Y. Shprits, S.R. Elkington, N.P. Meredith, D.A. Subbotin, Review of modeling of losses and sources of relativistic electrons in the outer belt II: local acceleration and loss. J. Atmos. Sol.-Terr. Phys. **70**, 1694–1713 (2008b). doi:10.1016/j.jastp.2008.06.014

A.L. Vampola, VLF transmission-induced slot electron precipitation. Geophys. Res. Lett. **4**, 569–572 (1977)

J.I. Vette, The AE-8 trapped electron model environment. NSSDC/WDC-A-R&S 91-24 (1991)